DEVELOPMENT OF A RADIANT POROUS BURNER WITH A COMBINED THERMAL AND FLUIDYNAMIC MECHANISM OF FLAME STABILIZATION

Rafael de Camargo Catapan
Department of Mechanical Engineering - Federal University of Santa Catarina – Florianópolis/SC
catapan@cet.ufsc.br

Fernando Marcelo Pereira
Department of Mechanical Engineering - Federal University of Santa Catarina – Florianópolis/SC
fernando@cet.ufsc.br

Amir Antonio Martins de Oliveira Júnior
Department of Mechanical Engineering - Federal University of Santa Catarina – Florianópolis/SC
amirol@emc.ufsc.br

Abstract. *Here we present a development of a radiating porous burner capable of operating at surface temperatures ranging from 500ºC to 1300ºC with high radiation efficiency. Burners with a large ratio between surface area and thickness are not easily stabilized resulting in a usually short operational range. The combination of thermal and fluidynamic stabilization mechanisms proved to be a simple and efficient way of increasing the operation range and led to a new and innovative design of porous radiating burners. Burners with different layers of silicon carbide (SiC) and zircon oxide (ZrO_2) ceramic foams operating with premixed methane and air were built and tested. The fuel equivalence ratio ranged from 0.35 to 0.65 resulting in total power between 60 kW/m^2 and 880 kW/m^2. For the SiC burners, the radiation efficiency varied between 20% and 35% and the surface temperatures between 450ºC and 900ºC. For the ZrO_2 burners, the radiation efficiency varied between 25% and 50% and the surface temperatures between 790ºC and 1170ºC. The results are summarized in a general regime diagram. The diagram provides information on flame stability, surface temperature and radiation efficiency and is presented as a tool for the design of applications. This development attends the demand of several industrial sectors for radiating burners of easy control and with ample range of operation.*

Keywords*: porous burner, radiant efficiency, stability diagram*

1. Introduction

There are several industrial sectors that use radiant heating in their productive processes. Yagoobi et al. (2000) studied the application of radiant burners in pulp drying in the paper industry. They found that using five sets of burners in the drying section the production speed can be increased in 30%, also improving the process and paper humidity control. Pereira et al. (2004) describe the application of radiant porous burners in continuous, or tunnel, kilns in the ceramic industry. Basically, these kilns use a large amount of air to increase the surface convective heat transfer to homogenize the heat transfer to the ceramic tiles. Large temperature gradients along the tiles and among tiles may cause large variations in surface finishing and lower dimensional control. The excess air, however, increases the power consumption, having a direct impact into the operational costs. Radiant porous burners may be used to control and direct the radiation field over the tiles surface achieving the same temperature homogenization with a smaller airflow.

In porous burners the combustion reaction takes place within a ceramic or metallic porous structure. The presence of the solid matrix promotes the heating of the incoming gas mixture by the heat transfer in the solid phase by conduction and surface radiation exchange. This preheating effect from sensible heat recirculation increases the local flame temperature and the rate of chemical reaction. Figure 1 presents a rendering of the gas and solid enthalpy across a flame within a porous medium, showing the increase of enthalpy in the flame zone as a result of sensible heat recirculation. The overall result is the increase of the stabilization range for laminar combustion, the possibility of combustion of low heat content fuels (or dilute mixtures) and smaller production of gas pollutants. The substrates of porous burners must have a low thermal expansion coefficient; they cannot suffer degradation in high temperature oxidant environments and must have high thermal conductivity and radiant emissivity in the temperature range of operation. Also, the combustion within the porous burner must be stable and uniform which is difficult to achieve in large surface area burners. The development of the substrate material and the design of stable large surface burners are the main difficulties in applying radiant burners to industrial applications.

This work focuses on achieving stable and uniform combustion in large surface burners. The first stabilization mechanism present in a radiant porous burner is the thermal stabilization imposed by the presence of a solid matrix, i.e., heat recirculation and heat loss to the surroundings. A second stabilization mechanism is present when two or more layers of different porous structures are used together. These two mechanisms are well known from the literature and are briefly discussed in the next paragraphs. A third stabilization mechanism is fluidynamic and is related to the

reactants injection in the burner. All these mechanisms are explored in this work to achieve stable and uniform combustion.

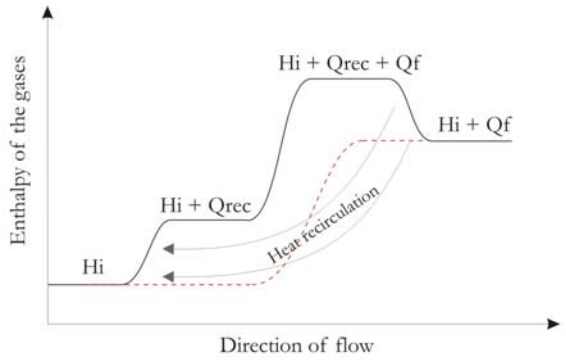

Figure 1. Rendering of the gas and solid enthalpy across a flame within a porous medium, showing the increase of enthalpy in the flame zone as a result of sensible heat recirculation, where Hi is the initial enthalpy, Qrec is the recirculated heat and Qf is the energy of the fuel.

Trimis and Durst (1996) showed that the rate of heat loss from the reaction zone increases as the pore size decreases, resulting in flame quenching as the pore size is decreased below a critical value. Therefore, when the combustion takes place within a double layer of ceramic foams, in which the layer located upstream has pore size below the critical value, there is a tendency of stabilization of the combustion front at the interface between the two layers. This is the usual mechanism for flame stabilization and has been explored by Pereira (2002) in the design of surface and volumetric porous burners. Hsu (1996) calls the layer with small pores as the preheating region (PR) and the layer with the larger pores as the stable-burning region (SBR).

Hsu (1996) analyzed the premixed methane and air combustion in different configurations of layered porous burner. One configuration has a third layer with small pores downstream the SBR. This new layer, called radiation-reflecting region (RRR), has the purpose of reflecting the escaping radiation intensity field back to the SBR. This allows for a second stable position for the flame at the downstream end of the SBR, moving the blow out limit to higher flame speed when compared to the double-layered burner. The temperatures within the porous burner also increase as a result of the larger heat recirculation. The measurements show that for the same equivalence ratio, the thermal degradation of the porous burner occurs at a flame speed about 5 cm/s smaller when the RRR is used.

The emissions achieved from these burners are well within present regulations. Khanna et al. (1994) measured the emission of CO and NO_x for premixed methane and air combustion in a double-layered porous burner at equivalence ratio between 0.60 and 0.87 and different flow rates. For a given equivalence ratio, they showed that the CO emission is minimum at intermediate values of flame speed. For an equivalence ratio of 0.60 and flame speed of 15 cm/s the CO emission was 45 ppm, while at 30 cm/s, the point of minimum emission level, it reached approximately 10 ppm. They observed also that the CO emission increases with equivalence ratio. In respect to NO_x, they observed that the burning of fuel lean mixtures decreases the temperature in the reaction zone then decreasing the emission of NO_x.

These ideas were tested using available ceramic foam plates and the measurements showed a great difficulty in achieving uniform combustion fronts within large surface area porous burner (Pereira, 2002). As it will be shown below, the flames had a macroscopic three-dimensional structure, presenting cold spots, where quenching would take place, while in other regions blowout or flashback would occur. As a result, the stability and control are compromised and the radiation intensity field from the burner is non-uniform. This led to the use of a third stabilization mechanism, which can be called to as a fluidynamics mechanism.

Here we report the development of a stable radiant burner using two layers of ceramic foams and a combined thermal and fluidynamic stabilization. The power, surface temperature, radiant efficiency and stability are characterized and the results are presented in a regime diagram, indicating the limits of stable operation. The regime diagram is constructed in a way of helping the designer to properly design the burner, or a set of burners, for a given application.

In the following, the burner design and characterization is described.

2. Experimental set-up and burner design

2.1. Experimental set-up

Figure 1 presents a schematic view of the apparatus for testing of radiant porous burners. Basically, it is composed of a burner section; air and fuel supply systems and measurement systems, including temperature measurement, infrared thermography, gas analyzer and data acquisition.

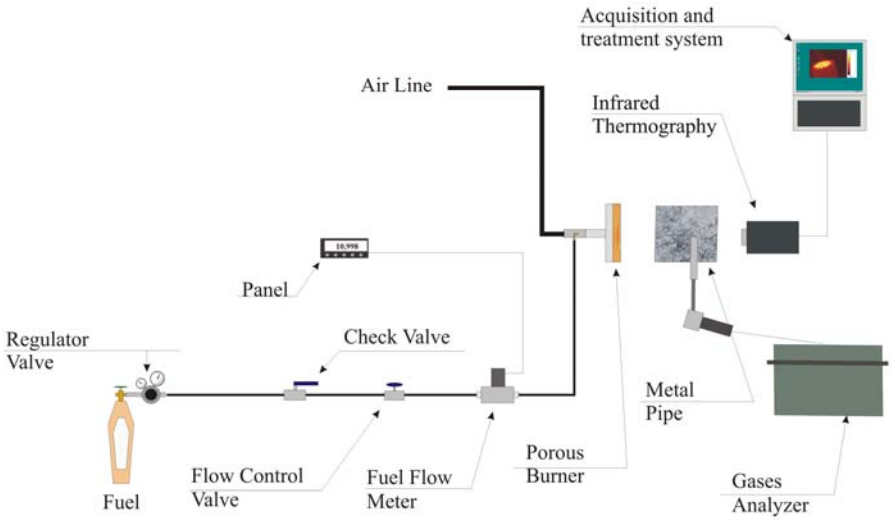

Figure 2. Schematic view the apparatus for testing of radiant porous burners.

Depending on the total power of the burner tested, two configurations are used. In the first, for burners with power between 20 kW/m^2 and 115 kW/m^2 and surface area less than 100 cm^2, a 5 bar compressed air line supplies the air flow, that ranges from 1x10^{-3} kg/s to 5x10^{-3} kg/s. The line is composed of a check valve, air flow control valve and an electronic flow meter (from Omega Engineering Inc.), with measurement range between 0 and 500 liters per minute (lpm) and measurement uncertainty of ± 0.75 lpm. In the second configuration, designed for burners with surface area under 225 cm^2 and power between 155 kW/m^2 and 880 kW/m^2, a centrifugal fan supplies the air flow. An alternate current frequency controller at the fan electrical power supply controls the fan speed providing air flows between 2.3x10^{-2} kg/s and 9x10^{-2} kg/s. At the fan outlet, a sphere valve allows for a second flow control and also as a safety shut off valve. An orifice plate flow rate meter is used to measure the air flow rate. The pressure drop across the orifice plate is measured using a differential pressure transducer (PX653- 25D5V, from Omega Engineering Inc.), with measurement range between 0 and 635 mmH_2O and uncertainty of 0.25%. The methane flow rate is measured by an electronic flow meter (from Omega Engineering Inc.) with the measurement range between 0 and 50 lpm and measurement uncertainty of ± 0.05 lpm. Type R (platinum and platinum + 13% rhodium) thermocouples insulated inside alumina beads are used to measure the temperature within the porous burner. These have measurement range between 50ºC and 1768ºC and measurement uncertainty of ± 4ºC. Values of temperature are recorded by an Agilent 34970 A data acquisition system interfaced to a personal computer. A thermography system Flir Systems model FLIR 500 measures the surface infrared radiation emission. A KANE model KM9106 gas analyzer is used for measurement of CO, CO_2 and NO_x mole fractions at the burner outlet. The estimated uncertainty in the mole fraction measurements is 1 ppm for CO, 0.1% for CO_2 and 5 ppm for NO_x.

A shielded and cooled probe is used to measure simultaneously the gas temperature and species mole fractions at the burner outlet. Figure 3 shows a schematic view of the probe. It is made from two concentric stainless-steel tubes connected to a small exhaust fan and having a K type thermocouple placed near the opening. Cooling water flows in the annulus between the two tubes. The fan takes the gas from the burner to the gas analyzer. The thermocouple is placed such that it is shielded from direct radiation from the burner surface.

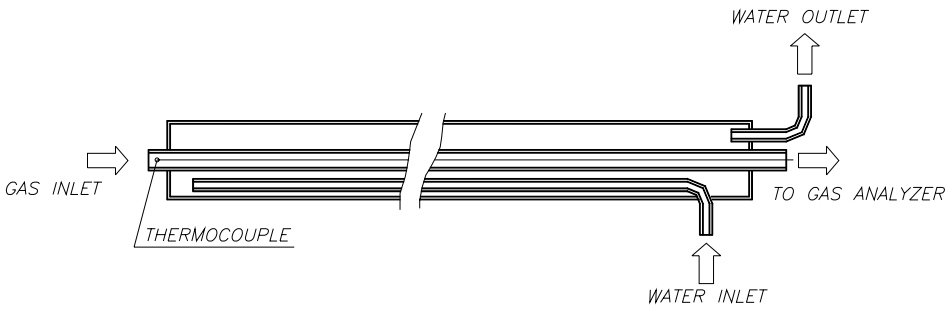

Figure 3. Schematic drawing of the cooled probe for gas temperature and species mole fraction measurements.

2.2. Experimental method

The experimental method used in this work follows Hsu et al. (1993). It consists of choosing a fuel equivalence ratio and a gas volumetric flow rate that allows for flame propagation within the porous burner. The flame stabilizes in the SBR in a region near the interface between the PR and the SBR. The equivalence ratio is slowly adjusted to the desired value and the volumetric flow rate is increased until the upper limit for flame propagation (the blowout limit) is reached. Then, the burner is reinitialized and the volumetric flow rate is decreased until the lower limit for flame propagation (the flashback limit) is reached. The procedure is repeated for each value of fuel equivalence ratio until the upper and lower flammability limits meet at the smaller possible fuel equivalence ratio. The larger possible fuel equivalence ratio is limited by the upper temperature limit for the porous matrix used. Here, the fuel equivalence ratio follows the usual definition as,

$$\phi = \frac{\left(\dot{m}_F \big/ \dot{m}_a \right)_a}{\left(\dot{m}_F \big/ \dot{m}_a \right)_S} \tag{1}$$

The flame speed (S_L) is calculated dividing the gas flow rate by the burner area. A flame is considered stable when the recorded temperatures within the porous burner vary by less than 10ºC in ten minutes. After finding a stable flame, an infrared image of the burner surface is recorded and the gas temperature and composition are measured. The blow off limit is identified as the flame speed beyond which the flame stabilizes outside the burner and is visually seen as a trembling blue flame at the burner surface. The flash back limit is defined as the flame speed for which the flame penetrates the preheating layer (PR), being identified by a sudden increase in the temperature recorded by the thermocouple placed upstream the PR layer.

For the gas temperature and composition measurement, a chimney is installed at the burner outlet and the probe is introduced at a distance of 10 cm above of burner surface. The chimney prevents the entrainment of ambient air in the gas flow out of the burner. During the measurement the temperature readings by the thermocouples within the porous burner are observed to detect whether the presence of the chimney has altered the combustion. The chimney is then removed and the procedure follows on to record the flammability limit for the next fuel equivalence ratio.

An estimate of measurement uncertainties resulted in ± 10 K for the temperature measurements, ± 1 mm for the dimensional linear measurements, ± 0.05 for emissivity values and ± 1.5% in fuel mass flow rate measurements. This leads to a maximum of ± 10% uncertainty in flame speed values. The measurements of flame speed and radiation output by the infrared camera are checked such that the global energy balance is satisfied. The difference, fewer than 10 %, is attributed to experimental uncertainty and peripheral heat loss.

2.3. Burner design

Three different burner designs have been tested. Two configurations have been developed based on the results reported by Hsu (1996). The first configuration is a square shaped with 100 by 100 mm, with a PR of 40 ppi (pores per inch) and 20 mm of thickness, a SBR of 10 ppi and 20 mm of thickness and a RRR with 40 ppi and 20 mm of thickness, as shown in figure 4. The second configuration is similar to the first one, but it has a SBR of 10 ppi and 40 mm of thickness and it does not have a RRR. Silicon carbide (SiC) porous foams are used (manufactured by Foseco Ind. e Com. Ltda.). They have 80% of volumetric porosity and a square shape with side equal to 100 mm, totalizing a radiating area of 100 cm^2. The foams are manufactured by Industrial and Commercial Foseco Ltda.

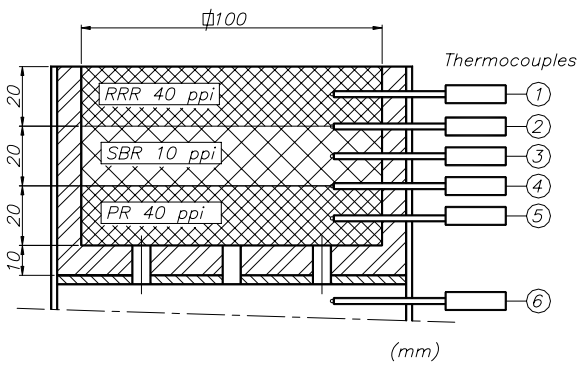

Figure 4. Schematic drawing of the silicon carbide, three-layer porous burner (configurations 1 and 2).

The third configuration is shown in Figure 5. It has two layers of zirconia (ZrO_2) porous foam (manufactured by Selee Corp.). The PR layer has 45 ppi, 80% of volumetric porosity and 20 mm thickness. The SBR layer is formed by two foams with 10 ppi, 80% of porosity each one and 10 mm of thickness. The ceramic foams have a square shape with 150 by 150 mm, totalizing a radiating area of 225 cm^2.

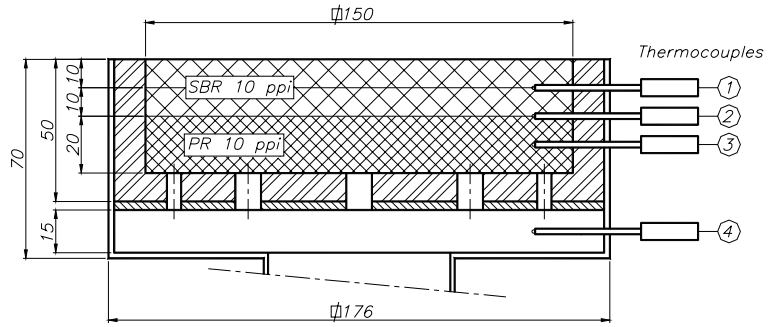

Figure 5. Schematic drawing of the zirconia, two-layer porous burner (configuration 3).

The ceramic plates are arranged inside a square box made of 3 mm thick stainless-steel plates. The interface between the foams and the steel plates is insulated with an alumina blanket, which is stable to temperatures up to 1470º. Underneath the PR layer there is a flow distributor made of a perforated stainless-steel plate. Six thermocouples in the first and second configuration and four thermocouples in the second configuration measure the temperature distribution along the porous foams. Thermocouples numbered 6 in Figure 4 and 4 in Figure 5 are used to detect flashback.

3. Results and Discussion

3.1. Preliminary tests

As mentioned above, it is difficult to obtain a homogeneous flame. As the control valves are actuated to stabilize the flame within the flammability region, the flame remains transient and develops a three-dimensional structure, as shown in Figure 6(a). In this condition, the radiation emitted by the flame is non-uniform and cold spots are visually observed over the burner surface. In these cold spots, there is extinguishment either by blow-off or by flash back, depending on the local value of the flow rate. Once a distributor plate is added, the flame stabilizes and a homogeneous surface radiation is obtained.

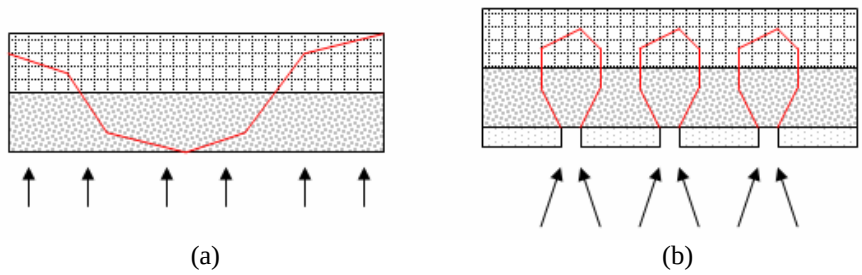

Figure 6 – Scheme of two burner configuration - the red lines represent the flame front: a) two ceramic plates and b) two ceramic plates plus a punched isolating plate.

The distribution plate has an array of circular holes, each with a determined diameter. The effect of the holes is shown in Figure 6(b). The holes direct the premixed methane and air flow to a few specific points under the PR layer. The pressure drop across the holes determines the amount of volumetric flow rate in each hole, which is a function of the hole diameter. Above each hole, a flame with an approximate axissimetric bell shape develops. The shape is not exactly axissimetric because of the flame interactions. The result is a practically uniform burner surface temperature. The advantage of this design in flame stabilization is that above each hole the flow expands and decelerates, originating a flame stretch, and the flame position stabilizes where the local flame velocity equilibrates the flow speed in a mode essentially like a Bunsen burner flame. Different distributor plates were used in the three designs. The sizes end distribution of the holes may be optimized to obtain a different surface temperature distribution, or to stabilize the burner into a different region in the flammability diagram.

In the following, the flammability results for the thermal and fluidynamic stabilized porous burners are presented in regime diagrams.

3.2. Regime diagram

3.2.1 Configurations 1 and 2

Figure 7 shows the regime diagram for configurations 1 and 2. This diagram summarizes the set of macroscopic thermal characteristics measured for the porous burner. The horizontal axis presents the fuel equivalence ratio and the vertical left axis presents the flame speeds. The right vertical axis shows the radiation efficiency. The inclined clashed lines in the diagram correspond to the mass flow rates of methane and air, which are proportional to the total burner power. The inclined lines inside the flammability region present the burner average temperature. Each point in the stability limits is measured, at least, three times. As expected, the flammability range increases when the fuel equivalence ratio increases. The upper and lower flammability limits meet at the low equivalence ratio limit. Stable combustion was achieved for equivalence ratios from 0.33 to 0.60. Above the equivalence ratio of 0.60, the burner temperatures reach values that may cause the degradation of the ceramic foam.

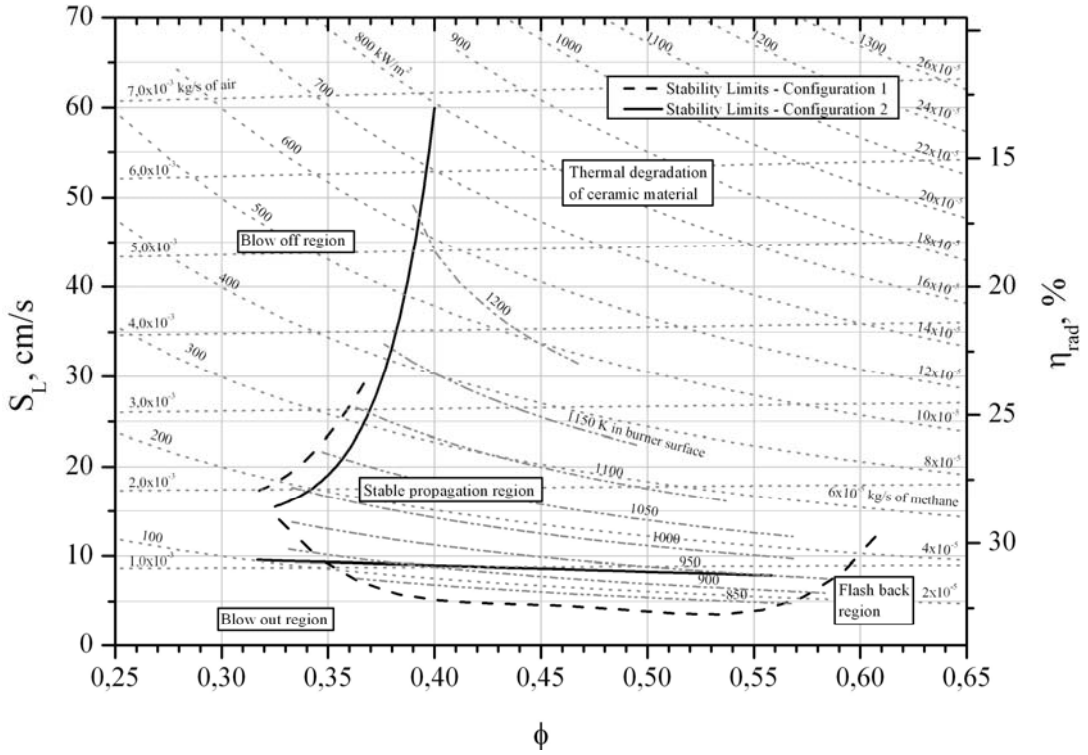

Figure 7. Regime diagram for configurations 1 and 2.

Outside the flammability region, extinguishment may occur by flash back, blow out and blow off. Above the upper limit, there is blow off, because the mixture flow rate exceeds the flame speed at some point in the burner. Below the lower limit, extinguishment may occur by flash back or blow out. In the flash back limit, the flame speed exceeds the flow speed and the flame moves upstream inside the PR layer. In the blow out limit, the flame is quenched because of excessive heat loss to the preheating region. We note that the lower limit of stability for both configurations remains approximately at 6 cm/s for configuration 1 and 10 cm/s for configuration 2 (for Φ between 0.40 and 0.55). Extinguishment by flash back was only observed for configuration 2 for Φ = 0.60. For configuration 1, only blow out was detected. We emphasize that this lower limit was only defined clearly for the burners with the distributor plate.

The use of a RRR layer (configuration 1) resulted in a wider stable region. The reduction of the lower limit occurs because the increased heat recirculation causes an increase in the internal temperatures. Then, the burner even working at lower powers, reaches high temperatures enough to sustain the flame. The minimum surface temperatures measured are 450ºC for configuration 1 and 570ºC for configuration 2. These low temperatures are suitable for low temperature applications, such as drying of organic material or paper drying. The increase in the upper limit occurs also because of the heat recirculation. An increase in the heat transfer back to the incoming mixture causes an increase in flame speed, resulting in higher upper flammability limit. The limit of thermal degradation for configuration 1 is reached at Φ = 0.40 with speed of 60 cm/s. In configuration 2, this limit was not reached. The use of the RRR layer has no effect in the lower value reached for the equivalence ratio, that is 0.33 for both configurations.

We note finally that in configuration 1 the burner operated in stable condition from 60 kW/m^2 to 600 kW/m^2, resulting in a power ratio of 1:10. In configuration 2, stable operation occurred from 100 kW/m^2 to 800 kW/m^2, a power ratio of 1:8.

3.2.1 Configuration 3

Figure 8 shows the regime diagram for the burner operating in configuration 3. The tests were done in the equivalence ratio region between 0.47 and 0.65.

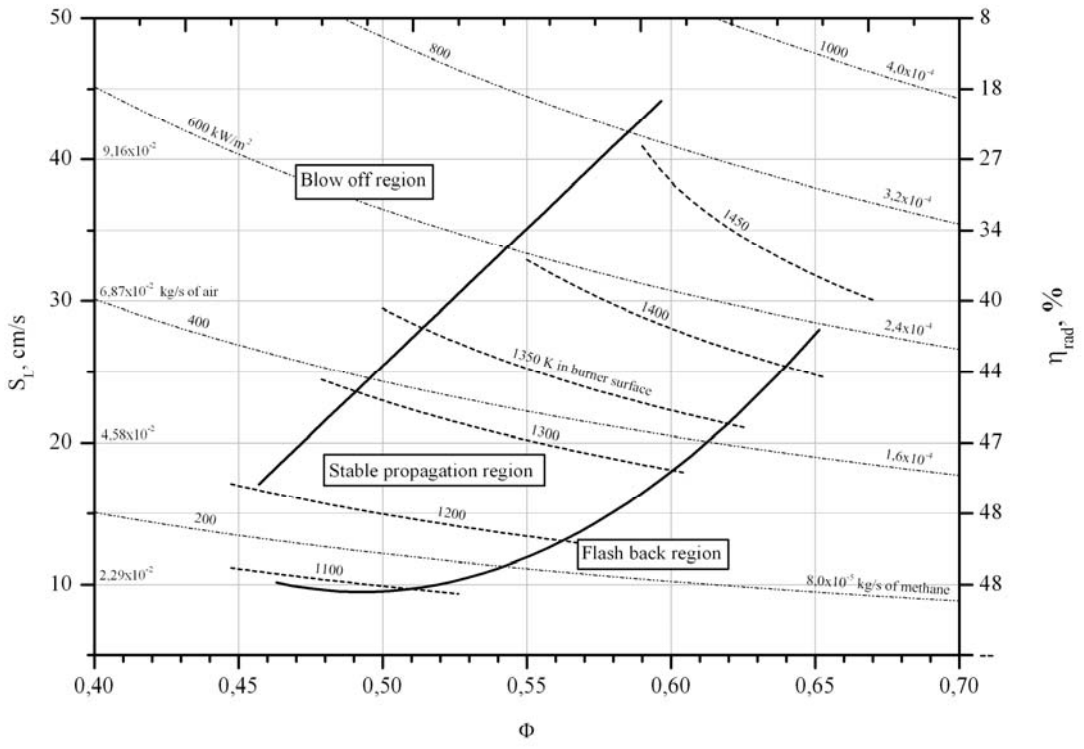

Figure 8. Regime diagram for configuration 3.

The surface temperature varied between 790ºC and 1170ºC. The total power varied between 155 kW/m^2 for a flame with Φ = 0.47 and S_L = 10 cm/s and 880 kW/m^2 for a flame with Φ = 0.60 and S_L = 45 cm/s, resulting in power ratio of 1:5. The burner did reach the thermal degradation limit for zirconia, which is estimated in 1600ºC, but tests above 880 kW/m^2 were not conducted due to safety reasons.

As before, the regime diagram present the mass flow rate of air and methane at each operating condition. Therefore, it is an easy task, to set up an operation point. That matches the requirements of a given application in terms of surface temperature, total power and radiation efficiency. Dynamic control is also possible, since the burner can switch freely between operating points within the stable operation region.

3.3. Radiation efficiency

The radiation efficiency of the burner is defined as ratio between the energy emitted by the burner through thermal radiation and the total energy released by the combustion process. Figure 9 shows the radiation efficiency as a function of the flame speed for different values of equivalence ratio for configuration 1 (Figure 9a) and configuration 3 (Figure 9b). With configuration 1 the radiation efficiency (η_{rad}) varied between 20% and 30%. Configuration 2 presented similar results. With configuration 3 the radiation efficiency varied between 25% and 50%. It is observed that for both configurations the radiation efficiency decreases with the increase in flame speed, as a result of the increasing importance of the convective thermal energy flow at the burner surface when compared to the radiative heat transfer. It is speculated that the optimization of the distribution plate to obtain stable flames at lower speeds may increase the radiation efficiency significantly. In Figure 9 we also observe that the equivalence ratio has a smaller effect in the radiation efficiency, and the effect observed is within the experimental uncertainty.

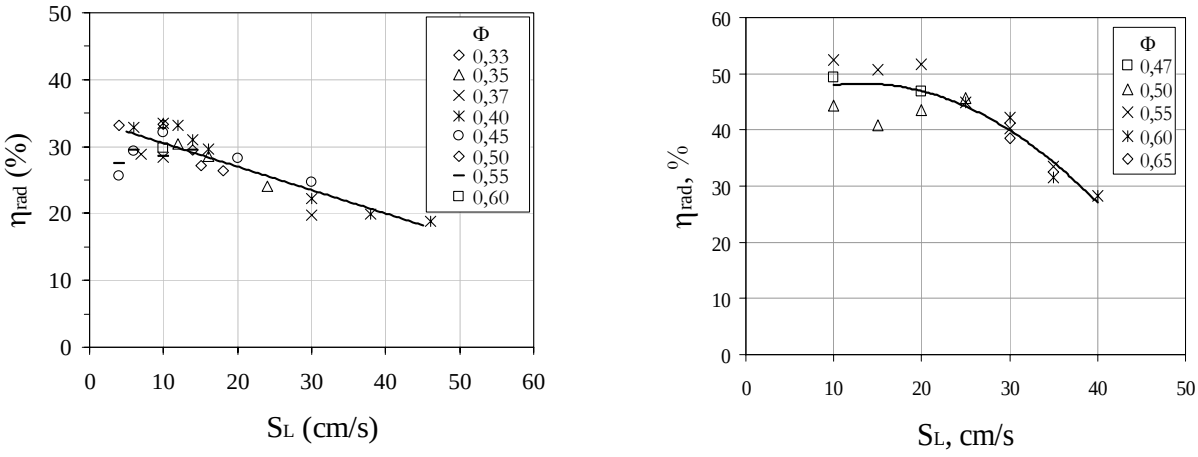

(a) (b)

Figure 9. Radiation efficiency as a function of the flame speed for different values of equivalence ratio for configuration 1 (Figure 9a) and configuration 3 (Figure 9b).

A curve fit for the points shown in Figure 9 results in

$$\eta_{rad} = -0{,}35 \times S_L + 34; \qquad for\ 6 \le S_L \le 46 \tag{2}$$

for configuration 1 and

$$\eta_{rad} = -0{,}029 \cdot S_L^{\,2} + 0{,}8 \cdot S_L + 43{,}1\ ; \qquad for\ 10 \le S_L \le 45 \tag{3}$$

for configuration 3.

3.4. Surface temperature

Figures 10(a) and 10(b) shows the infrared thermography image of burner configuration 3 operating with Φ = 0.45 and S_L = 15 cm/s and with Φ = 0.60 and S_L = 40 cm/s, respectively. The bright spots identify the mixture injection points. In both figures the surface temperature varies across the surface by less than 100ºC.

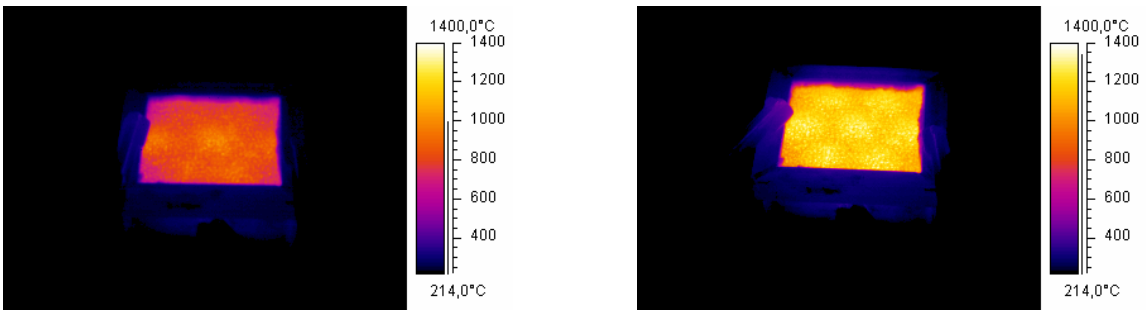

(a) (b)

Figure 10. Infrared thermography image of the burner in configuration 3 for (a) Φ = 0.45 and S_L = 15 cm/s and (b) Φ = 0.60 and S_L = 40 cm/s.

3.5. Emissions of CO and NOx

Emissions of CO were measured for configurations 1 and 3 and the results are shown in Figure 11(a) and 11(b), respectively.

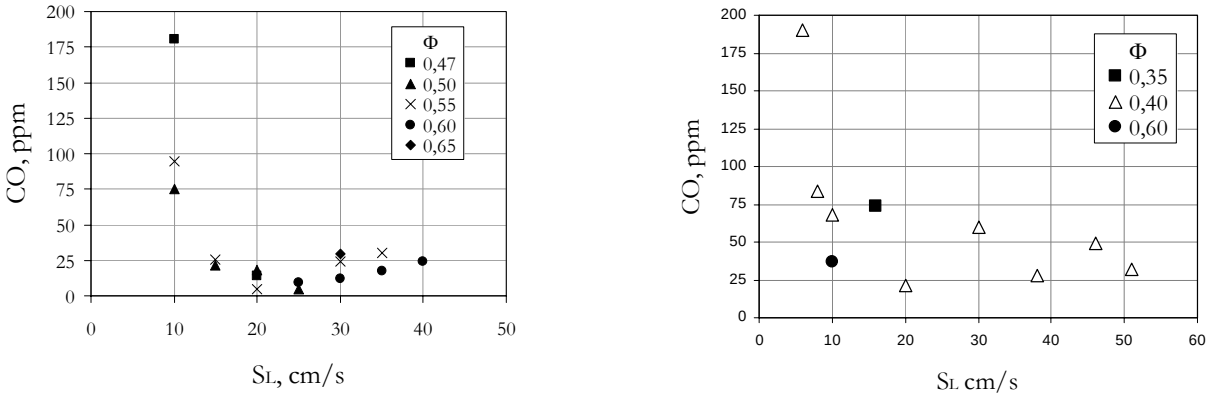

(a) (b)

Figure 11. Emission of CO (corrected to 5% of O_2) for different equivalence ratios as a function of flame speed for configurations (a) 1 and (b) 3.

It is observed that the CO emission was below 50 ppm for configuration 1 and 75 ppm for configuration 3 for almost all of the points measured. The few measurements in low flame speed revealed higher emission of CO, between 40 ppm and 180 ppm. These points are close to the inferior limit of stability, where the flame approaches the blow out limit and the flame temperature is lower.

The NO_x emissions were always within the gas analyzer resolution. Only for the highest Φ studied (0.65) a 5 ppm level of NO_x was detected for S_L = 30 cm/s. This overall low level of NO_x emission is related to the low temperatures achieved since the mixtures were all fuel lean (Khanna et al., 1994).

4. Conclusions

A radiant porous burner capable of operating at surface temperatures ranging from 500ºC to 1300ºC with high radiation efficiency is developed using a combination of thermal and fluidynamic stabilization mechanisms. The thermal characteristics of the burners developed are measured and summarized in a general regime diagram. The diagram provides information on flame stability, surface temperature and radiation efficiency and is designed as a tool for applications. This development attends the demand of several industrial sectors for radiant burners of easy control and with ample range of operation.

The main findings can be summarized as

1. The use of a distribution plate underneath the ceramic foams extends the burner stability limits. This method of flame stabilization differs from the commonly used mechanism in porous burners reported before.
2. Three basic configurations were tested. In configuration 1 and 2 the radiation efficiency (η_{rad}) varied between 20% and 30%. In configuration 3 the radiation efficiency varied between 25% and 50%. For all configurations the radiation efficiency decreases when the flame speed is increased. It is speculated that the optimization of the distribution plate to obtain stable flames at lower speeds may increase the radiation efficiency significantly.
3. The combustion stability of configurations 1 and 2 is limited for low values of flame speed by blow out, while for configuration 3, it is limited by flash back.
4. In configuration 1, the radiation-reflecting region (RRR) decreased the lower flammability limit by 6 cm/s when compared to configuration 2, without RRR. This effect can be assigned to the greater heat recirculation that results in an increase of the internal temperature of the burner, allowing the combustion to occur at lower power.
5. The use of the RRR radiation-reflecting region (RRR) does not decrease the inferior limit of flammability and therefore is not an alternative for the combustion of low energy content fuels. The inferior limit of inflammability remained at 0.33 for both configurations 1 and 2.
6. A regime diagram was developed based on the measurements for each configuration. The regime diagrams present the mass flow rate of air and methane at each stable operating condition. Therefore, it is an easy task, after the diagram is available, to set up an operation point. This operation point is established such that the total power and the radiation efficiency, or the surface temperature, are set to match the requirements of a given application. Dynamic control is also possible, since the burner can switch freely between operating points within the stable operation region.
7. The CO emission was below 50 ppm for configuration 1 and 75 ppm for configuration 3 for almost all of the flame speed range. Only close to the inferior limit of flammability there was an increase of CO levels up to 180ppm.

This occurs because of the lower flame temperature allowing for incomplete combustion at cold spots within the burner. The measured levels of NOx remained under the analyzer resolution, due to the fuel lean mixtures burned.

The application of the radiant burners developed to industrial processes is under way. We expect soon to report the results relating to these applications.

5. Acknowledgements

The authors gratefully acknowledge the financial support of RedeGasEnergia (Petrobras, TBG and SCGás) and FINEP-FNDCT through a 2001 CTPETRO research grant and the program ANP PRH-09/MECPETRO for the constant support in the form of undergraduate and graduate scholarships. The many contributions of the undergraduate students Andrio Angioletti, Newton Júnior Hissanaga and Marcelo Fonseca do Carmo and the comments by Dr. Ricardo Serfaty (CENPES-PETROBRÁS) are also greatly appreciated.

6. References

Catapan, R. C., Pereira, F. M., Oliveira, A M., “Relatório de caracterização de queimadores porosos radiantes de baixa temperatura”, Tecnical report, UFSC, RedeGás Energia, 2004.

Catapan, R. C., Pereira, F. M., Oliveira, A M., “Relatório de caracterização de queimadores porosos radiantes de alta temperatura”, Tecnical report, UFSC, RedeGás Energia, 2004.

Hsu, P. F., “Experimental study of the premixed combustion within the nonhomogneous porous ceramic media”, National Heat Transfer Conference, Vol.6, ASME 1996.

Hsu, P. F., Evans, W. D., Howell, J. R., “Experimental and numerical study of premixed combustion within nonhomogeneous porous ceramics”, Combust. Sci. and Tech., Vol. 90, pp. 149-172, 1993.

Khanna, R., Goel, R., Ellzey, J. L., “Mesurements of emissions and radiation for methane combustion within a porous medium burner”, Combust. Sci. and Tech., Vol. 99, pp. 133-142.

Pereira, F. M., 2002, “Medição de características térmicas e estudo do mecanismo de estabilização de chama em queimadores porosos radiantes” ”, in Portuguese, M.Sc. Thesis, UFSC, 145 p.

Pereira, F. M., Catapan, R. C., Oliveira, A M., “Relatório de Análise Técnico-Econômica de Aplicações para Queimadores Porosos Radiantes”, Tecnical Report, UFSC, RedeGásEnergia, 2004.

Trimis, D., Turst, F., “Combustion in a porous medium – advances and applications” Combust. Sci. and Tech. Vol. 121, p.153-168, 1996.

Yagoobi, J. S., Sikirica, S. J., Ricks, M. R., “On-line pre-heating-drying of paper sheet with gas-fired infrared emitters”, APPI Vancouver, 2000,.

7. Responsibility notice

The authors are the only responsible for the printed material included in this paper.